Ideal strength of bcc molybdenum and niobium

Weidong Luo,[1,2,*] D. Roundy,[1,2] Marvin L. Cohen,[1,2] and J. W. Morris, Jr.[3,2]
[1]*Department of Physics, University of California at Berkeley, Berkeley, California 94720*
[2]*Materials Sciences Division, Lawrence Berkeley National Laboratory, Berkeley, California 94720*
[3]*Department of Materials Science and Engineering, University of California at Berkeley, Berkeley, California 94720*
(Received 11 December 2001; revised manuscript received 30 April 2002; published 18 September 2002)

The behavior of bcc Mo and Nb under large strain was investigated using the *ab initio* pseudopotential density-functional method. We calculated the ideal shear strength for the $\{211\}\langle 111\rangle$ and $\{011\}\langle 111\rangle$ slip systems and the ideal tensile strength in the $\langle 100\rangle$ direction, which are believed to provide the minimum shear and tensile strengths. As either material is sheared in either of the two systems, it evolves toward a stress-free tetragonal structure that defines a saddle point in the strain-energy surface. The inflection point on the path to this tetragonal ''saddle-point'' structure sets the ideal shear strength. When either material is strained in tension along $\langle 100\rangle$, it initially follows the tetragonal, ''Bain,'' path toward a stress-free fcc structure. However, before the strained crystal reaches fcc, its symmetry changes from tetragonal to orthorhombic; on continued strain it evolves toward the same tetragonal saddle point that is reached in shear. In Mo, the symmetry break occurs after the point of maximum tensile stress has been passed, so the ideal strength is associated with the fcc extremum as in W. However, a Nb crystal strained in $\langle 100\rangle$ becomes orthorhombic at tensile stress below the ideal strength. The ideal tensile strength of Nb is associated with the tetragonal saddle point and is caused by failure in shear rather than tension. In dimensionless form, the ideal shear and tensile strengths of Mo ($\tau^* = \tau_m / G_{111} = 0.12$, $\sigma^* = \sigma_m / E_{100} = 0.078$) are essentially identical to those previously calculated for W. Nb is anomalous. Its dimensionless shear strength is unusually high, $\tau^* = 0.15$, even though the saddle-point structure that causes it is similar to that in Mo and W, while its dimensionless tensile strength, $\sigma^* = 0.079$, is almost the same as that of Mo and W, even though the saddle-point structure is quite different.

DOI: 10.1103/PhysRevB.66.094110 PACS number(s): 62.20.Fe

I. INTRODUCTION

The ideal strength is the stress required to yield or break a perfect crystal.[1,2] The most important feature of the ideal strength is that it sets an upper bound on the attainable stress. Mobile dislocations, grain boundaries, cracks, and other microstructural features may significantly change the strength of a real crystal, but they can never raise it above its ideal value.

The upper limit of strength is of obvious interest in materials science, and theorists have attempted to compute it from atomic models since at least the 1920s.[1,3,4] These early models assumed simple analytic forms for the stress-strain relation at large strains that made it possible to express the ideal strength in terms of experimental values of the elastic moduli. Later, in the 1970s and 1980s, semiempirical pair potential and embedded atom models were used to study the large strain behavior of bcc and fcc materials.[5–7] These studies helped to clarify the generic behavior of materials under large strain, but because the models used are based on fits to small strain behavior (e.g., the elastic constants), their quantitative accuracy at large strains is uncertain. Recently, *ab initio* methods have been used to calculate large strain behavior. These methods are not based on experimental measurements. They are equally valid at all strains and have proven successful in computing the ideal strength.[8–15]

The more sophisticated computations of the ideal strength have been accompanied by (and have contributed to) a clearer understanding of the meaning of the term.[16] When an infinite, perfect crystal is subjected to an increasing stress it responds elastically until the stress becomes so great that the lattice becomes unstable. This stress is the ideal strength. At its ideal strength the crystal necessarily fails, either by breaking (fracture), shearing into a deformed replica of itself (plastic deformation), or shearing into some new crystal structure (martensitic transformation). The specific mode of failure is a complex problem in molecular dynamics, since it depends on precisely how the lattice atoms move once the instability has set them free. However, assuming that we can ignore phonon-induced instabilities, the elastic stability limit is a problem in lattice statics that can be attacked with available theoretical tools.

Even in the quasistatic case the meaning of the ideal strength has subtle features.[16] Three are particularly important. The first concerns the boundary condition assumed for the problem. As Hill has pointed out,[17,18] the conditions of elastic stability for a material under load are sensitive to the behavior of the loading mechanism. This problem can be avoided by controlling the displacement, rather than the load, and defining the ideal strength as the load that produces the critical displacement at which the crystal becomes unstable with respect to internal displacements. The second concerns the direction of the instability. It sometimes happens that a given displacement (for example, an uniaxial tension) triggers elastic instability with respect to a very different displacement (for example, a orthogonal shear). It follows that all possible responses must be considered to identify the limit of strength. Third, the ideal strength is a highly anisotropic function of the displacement. It is significantly different for tension and shear and, ordinarily, depends strongly on the particular direction of tension or plane and direction of shear.

Many of the salient features of the ideal strength, including its anisotropy, can be understood from symmetry considerations. Finite strain can transform a crystal structure into itself or into an alternate symmetric structure. In bcc, for example, a homogeneous shear in the system $\{011\}\langle 100\rangle$ periodically regenerates bcc, while a homogeneous strain in relaxed tension along $\langle 100\rangle$ creates a tetragonal structure that may eventually become face-centered cubic (fcc), then tetragonal again. It follows that the plot of energy as a function of the six-dimensional strain is corrugated and punctuated with minima. The most favorable strain path that connects the starting structure to a nearby minimum necessarily passes through a state of maximum energy at a saddle point (mountain pass) on the energy surface. The relaxed, minimum-energy structure sits in a valley on the energy surface that is connected to other valleys by paths that pass through saddle points of this type.

The structures of the states at the saddle points (the ''saddle-point structures'') are particularly instructive in understanding the ideal strength for simple load configurations such as uniaxial tension or shear.[2,5,10,19] When a perfect crystal is loaded in uniaxial tension or balanced shear under displacement control, one strain is controlled while the other five independent strains adjust to minimize the energy. The strain path naturally evolves toward a saddle point in the energy surface. The stress that is associated with a particular strain is proportional to the derivative of the energy with strain. It follows that as a crystal is deformed from its equilibrium structure toward a saddle-point in the energy surface the stress increases, passes through a maximum, and returns to zero when the saddle-point structure is reached. The maximum stress is the ideal strength, and is associated with the inflection point in the curve of energy as a function of strain along the strain path toward the saddle point.[2]

Note that, unless the crystal is artificially constrained, the saddle-point structure is never reached. The crystal becomes elastically unstable and fails at its ideal strength, at roughly one-half the saddle-point strain. However, the saddle-point structure strongly affects the strain path and strongly influences the ideal strength. In fact, in most of the cases studied to date,[2,15,20] the ideal shear and or tensile strength can be approximated rather well by assuming a sinusoidal stress-strain relation that has the initial slope set by the appropriate elastic constant and returns to zero at the appropriate saddle-point strain.

In general, there are very few stress-free structures that can serve as saddle points, and most of these are determined by symmetry. Examples include the cubic structures, which are stress-free in simple crystals. Also, there is ordinarily one stress-free body-centered (or, equivalently, face-centered) tetragonal structure.[19] Because there are so few stress-free structures, the deformation paths generated by geometrically different stress states often pass through the same saddle point. Thus, an understanding of the few available stress-free states can provide a very general picture of the sources of the ideal strength.

In the present paper, we use the *ab initio* pseudopotential density-functional method to calculate the ideal tensile and shear strengths of Mo and Nb in tension and shear, and investigate the saddle-point structures that are responsible for the elastic instabilities that set the ideal strength. This research on Mo and Nb continues our exploration of the ideal strengths of bcc metals such as the prior work on W (Ref. 15) and concurrent work on Fe (Ref. 20). Both Mo and Nb have the bcc crystal structure and are similar in many of their physical properties, but there are intriguing differences in their elastic properties. In particular, the ratio of the shear and bulk moduli in Nb is much smaller than in Mo. This difference suggests that Nb is more likely than Mo to fail in shear rather than cleavage when stressed to the limit of its strength[21] (in fact, qualitative models suggest that Nb may have the best inherent ductility of all the bcc transition metals). It follows that Nb and Mo may have very different failure modes at large strain.

As we shall show below, there are only two relevant saddle-point structures in Nb and Mo (and, by inference, in other bcc structures): the face-centered cubic structure, and a body-centered tetragonal (bct) structure. The ideal shear strengths for the slip systems commonly found in bcc metals: $\{211\}\langle 111\rangle$ and $\{011\}\langle 111\rangle$, are nearly the same and are due to shear instabilities associated with the bct saddle-point structure. The ideal tensile strength for the weak direction $\langle 100\rangle$ in bcc is the result of a competition between the instabilities associated with the bct and fcc saddle-point structures, both of which lie on the $\langle 100\rangle$ tensile path. The fcc saddle-point governs the tensile strength of Mo, as it does for other common bcc metals such as W (Ref. 15) and Fe (Ref. 20) and appears to be the source of the $\{100\}$ cleavage that is common in bcc. However, the bct saddle point governs the $\langle 100\rangle$ tensile strength of Nb. The associated failure mode is an elastic instability with respect to shear on the system $\{211\}\langle 111\rangle$. This result suggests that Nb, unlike other common bcc metals, is inherently ductile when pulled in uniaxial stress.

II. METHOD

In the present paper, we use the *ab initio* pseudopotential density-functional method as employed in Refs. 11 and 15. The ideal strength is calculated by straining the crystal incrementally. At each step, the crystal is relaxed until all of the stresses orthogonal to the applied stress (for both shear and tensile stress) are reduced to zero. This produces a curve of energy versus strain, and a related curve of stress versus strain. The first maximum in the stress-strain curve is the ideal strength for this strain path provided no other instabilities occur before reaching it. The first zero reached along the stress-strain curve is the first maximum in the energy-strain relation along the relaxed (minimum-energy) path, and is, hence, a saddle point in the hypersurface of energy as a function of strain. The associated structure is the ''saddle-point structure'' that governs the ideal strength.

The total energy is computed as a function of strain using the local-density approximation (LDA) pseudopotential total-energy scheme with a plane-wave basis set.[22–25] We relax the structures using a quasi-Newton method[26] to minimize the energy. A plane-wave energy cutoff of 60 Ry is chosen, with a k grid of $16\times16\times16$ points in the full Bril-

TABLE I. The calculated ideal shear strength of Mo and Nb. The values for $\{211\}\langle 111\rangle$ shear strength and $\{011\}\langle 111\rangle$ shear strength are similar.

	Mo	Nb
$\tau_{m\{211\}}$(GPa)	15.8	6.4
$\tau_{m\{011\}}$(GPa)	16.1	7.6
G_{111}(GPa)	136	42.5(expt.)[27]
τ_m/G_{111}	0.116, 0.118	0.15, 0.18

louin zone. Using these parameters, we obtain equilibrium lattice constants for Mo and Nb of 3.17 and 3.30 Å, which are within 1% of the experimental values. The calculated bulk moduli are 283 and 195 GPa, respectively, which are around 10% greater than the experimental values of 264 and 170 GPa.[27] This result is typical of the LDA, which tends to overbind. For the Young's modulus in the $\langle 100\rangle$ direction and the shear modulus relevant to shear in the $\langle 111\rangle$ direction, we obtain agreement with experiment better than 8%, with the exception of the shear modulus of Nb. Our calculation of the shear modulus of Nb is 30% lower than the experimental value, so we use the experimental modulus when calculating the dimensionless shear strength of Nb, as indicated in Table I.

For finite deformation, there is some ambiguity in the definition of the strain. For the tensile strain, we find it convenient to use the engineering strain ϵ, for which the tensile stress σ is

$$\sigma_{\text{tensile}}=\frac{1+\epsilon}{V(\epsilon)}\frac{dE}{d\epsilon}, \tag{1}$$

where E is the strain energy and $V(\epsilon)$ is the volume at a given engineering strain. For the shear strain, it is convenient to use the true strain, as defined in Ref. 11. This strain is numerically very similar to the engineering strain, but has the advantage that one can calculate the shear stress τ from the energy versus strain curve via the equation

$$\tau_{\text{shear}}=\frac{1}{V(\gamma)}\frac{dE}{d\gamma}, \tag{2}$$

where γ now represents the true shear strain, while the other symbols are as defined above.

III. RESULTS

A. Ideal shear strength

The $\{211\}\langle 111\rangle$ shear is shown in Fig. 1. Figure 1(a) is a drawing of the cubic cell in the bcc structure with the $(1\bar{1}0)$ and $(\bar{1}\bar{1}2)$ planes shown. The initial (unsheared) atomic configurations in these planes are given by the solid symbols in Figs. 1(b) and 1(c), respectively. The circles give the atom positions in the plane while the diamonds label positions above the plane. The [111] direction of shear is to the right. When the atom represented by the solid diamond moves one third of the edge length to the position of the gray diamond, the structure returns to bcc. The intermediate structure indicated by the hollow symbols has the same symmetric relation to the initial and final bcc structures. It follows that the shear stress vanishes for this state. If all other stresses are also relaxed, this is the configuration of the saddle point for $\langle 111\rangle$ shear. If there were no relaxation, the shear strain to the saddle point would be $\gamma_t=\sqrt{2}/4\approx 0.35$ (as discussed previously in Refs. 21 and 15, on the basis of a slightly different geometric argument). The stress-free saddle-point structure is bct.

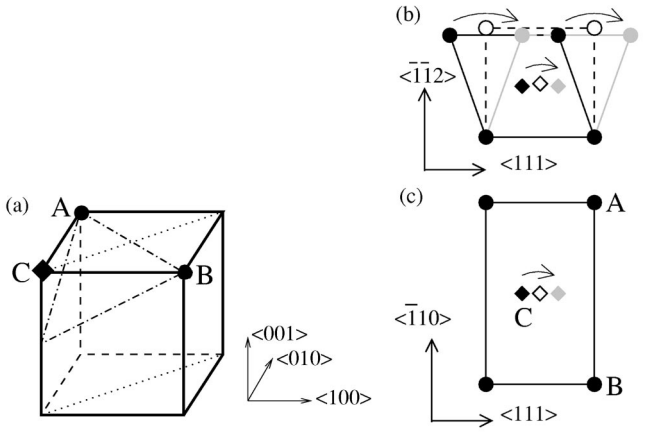

FIG. 1. The $\{211\}\langle 111\rangle$ shear in the bcc structure: (a) the bcc cubic cell showing the $(1\bar{1}0)$ plane (dotted line) and $(\bar{1}\bar{1}2)$ plane (dot-dashed line); (b) the atomic configuration in the $(1\bar{1}0)$ plane; and (c) the atomic configuration in the $(\bar{1}\bar{1}2)$ plane. The circles mark atom positions within the plane and the diamonds show positions above the plane. The solid black symbols and solid lines are the initial atom positions and cell edges. The solid gray symbols are the atom positions after shear has returned the structure to bcc. The hollow symbols and dashed lines show the tetragonal saddle-point structure.

To fix the actual configuration of the saddle-point structure, note that the intermediate tetragonal structure has two degrees of freedom; it can differ from the bcc parent in both volume and tetragonality (as given by the axial ratio, c/a). These parameters have values that minimize the energy. Our calculations show that the volume change is about 2% for both materials: 2.1% for Mo and 1.9% for Nb. The tetragonalities (c/a) with respect to the bcc ground state are, respectively, 1.73 for Mo and 1.81 for Nb.

The $\{011\}\langle 111\rangle$ shear differs from the $\{211\}\langle 111\rangle$ shear in that the lattice relaxes significantly during shear. This relaxation is necessary in order to return to the bcc structure at a strain of $\gamma\sim 0.60$. It also has the consequence that the $\{011\}$ shear path passes through the same tetragonal saddle-point structure that is reached by shear on $\{211\}$. The evolution of the structure during shear is illustrated in Figs. 2(a) and 2(b). The initial configuration is indicated by the solid black symbols. The gray symbols show the configuration after the shear has carried the crystal into a rotated bcc structure, a process that is accompanied by a substantial relaxation in the slip plane. The saddle-point structure is marked by the hollow symbols. This structure is tetragonal, and is identical to that shown for the $\{211\}\langle 111\rangle$ shear in Fig. 1. Note that the $\{011\}$ plane shown in Fig. 2 is also a $\{011\}$

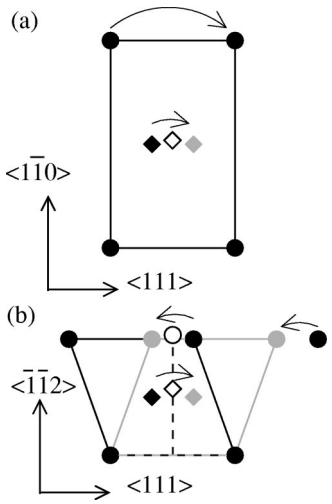

FIG. 2. The $\{011\}\langle 111\rangle$ shear in the bcc structure: (a) the atomic configuration in to the $(11\bar{2})$ plane and (b) the atomic configuration in to the $(\bar{1}10)$ plane. The circles label atom positions within the plane and the diamonds show the positions above the plane. The solid black symbols and solid lines are the initial atom positions and cell edges. The solid gray symbols are the atom positions after shear has returned the structure to bcc. The hollow symbols and dashed lines show the tetragonal saddle-point structure.

plane in the bct saddle-point structure. However, the $\langle 111\rangle$ direction in the parent bcc is a $\langle 100\rangle$ direction in the bct cell.

Figure 3 shows the energy as a function of strain for the $\{211\}\langle 111\rangle$ and $\{011\}\langle 111\rangle$ shears in the two materials. The maximum energy for both slip systems is the energy of the tetragonal saddle-point structure and is, therefore, the same for both slip systems: 0.35 eV for Mo and 0.15 eV for Nb. However, the shear strain γ_t required to reach the saddle-point is somewhat different for the two systems because of their different relaxations. For {211} slip, the saddle-point strain is very close to the unrelaxed value 0.35, but for {011} slip the saddle point is reached sooner, at $\gamma_t \sim 0.30$ for both Mo and Nb.

Figure 4 shows the shear stress-strain curves, which are obtained by differentiating the energy strain curves according

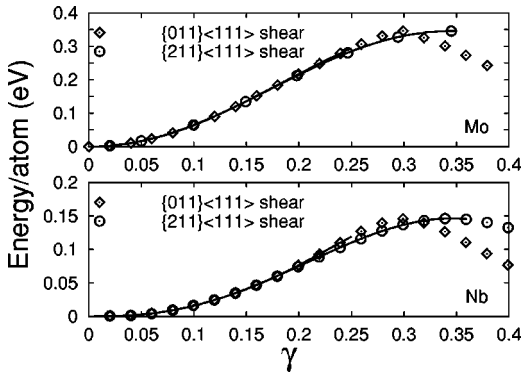

FIG. 3. The energy as a function of shear strain for Mo and Nb. The diamonds refer to shear on the {011} plane, the circles refer to shear on {211}. Since the structure returns to bcc at large strain, the curves are symmetric with respect to their maximum energy points.

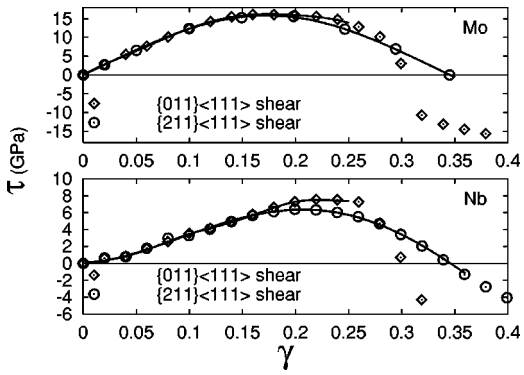

FIG. 4. Shear stress as a function of strain for Mo and Nb. The diamonds indicate the results for shear on the {011} plane, and the circles indicate the results for shear on the {211} plane.

to Eq. (2). The maximum in the shear stress-strain curve is the ideal shear strength provided no other instabilities occur before reaching it; a perfect crystal is unstable with respect to deformation in shear when this stress is exceeded. The calculated values of the shear strength are tabulated in Table I.

The stress-strain curves for the two slip systems coincide in the small strain limit, since their slopes are determined by the shear modulus, which can be expressed in terms of elastic constants C_{ij}

$$G_{\{011\}\langle 111\rangle} = G_{\{211\}\langle 111\rangle} = \frac{3C_{44}(C_{11}-C_{12})}{C_{11}-C_{12}+4C_{44}}. \qquad (3)$$

However, they differ at larger strains, and between materials. The stress-strain curve for {211} shear in Mo is almost a perfect sinusoid, with a critical strain γ_c near $0.17(=\gamma_t/2)$. The ideal shear strength $\tau_m = 15.8$ GPa $= 0.12\ G_{111}$. The stress-strain curve for {011} shear in Mo deviates from the sinusoidal form, but the deviation only becomes significant after the shear instability has been passed. The ideal shear strength for this system is $\tau_m = 16.1$ GPa, which is almost identical to that on {211}. The Nb stress-strain curves are less simple. In the $\{211\}\langle 111\rangle$ system, the shear stress-strain curve of Nb is skewed from the sinusoidal shape toward higher strain, and does not reach its peak until $\gamma_c \sim 0.2$. The shear strength $\tau_m = 6.4$ GPa $= 0.15\ G_{111}$; Nb has a higher dimensionless shear strength than Mo, though its actual strength is lower. Also, the stress-strain behavior of Nb on {011} is more obviously different from that on {211} than was the case for Mo. In Nb, the shear stress-strain curve for the {011} plane begins to deviate from the {211} curve before the peak stress is reached, and rises to a higher strength $\tau_m = 7.6$ GPa $= 0.18\ G_{111}$ at a slightly higher instability strain $\gamma_c \sim 0.22$.

B. Ideal tensile strength

By symmetry and prior calculation[15] the ideal tensile strength of a bcc metal is expected to have its minimum value for tension in the $\langle 100\rangle$ direction. We therefore calculated the strength of Mo and Nb for this case. The results are shown in Figs. 5 and 6, which are plots of the energy and

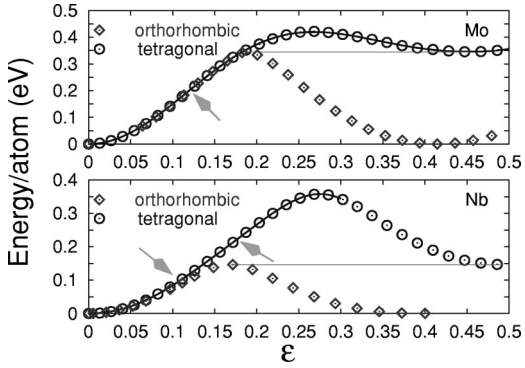

FIG. 5. Energy as a function of relaxed ⟨100⟩ tensile strain for Mo and Nb. The diamonds indicate the orthorhombic path, and the circles indicate the tetragonal path. The maximum of the orthorhombic path has the same energy as the local minimum of the tetragonal path, since they correspond to the same tetragonal saddle-point structure.

stress as functions of relaxed tensile strain (uniaxial stress) along [001]. The ideal tensile strengths are tabulated in Table II.

The response to tensile stress is also governed by the stress-free structures that provide saddle points in the strain-energy surface. If we maintain tetragonal symmetry by forcing homogeneous deformation in the *x*-*y* lattice plane as we pull in the [001] *z* direction (the Bain path), then the saddle point is the fcc structure for both materials. Along this path, the lattice is body-centered tetragonal (bct). As shown in Fig. 7(a), the unit cell can be drawn equally well as face-centered tetragonal (fct). Assuming constant volume, the strain at which the bcc cell assumes the fcc structure (the Bain strain) is $\epsilon_B = \sqrt[3]{2} - 1 = 0.260$. When the cell is constrained to be tetragonal, our calculations show that the volume change is less than 5% for Mo and less than 6% for Nb along this path. The strains at which bcc Mo and Nb assume the fcc structure are, respectively, 0.267 and 0.274, which are remarkably close to the value of ϵ_B for the volume-conserving Bain path.

If the [001] strain is continued past the fcc saddle point, while preserving tetragonal symmetry, it eventually reaches a stress-free tetragonal structure. This is the same bct structure

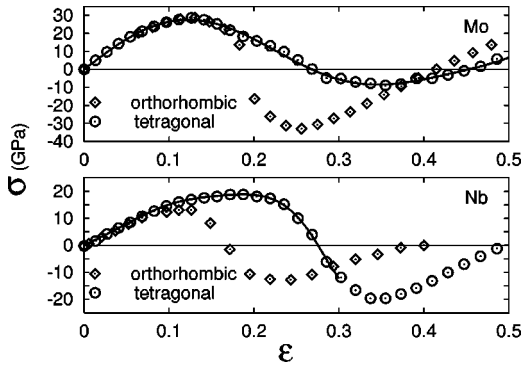

FIG. 6. Stress-strain curves for relaxed tension as a function of strain for relaxed tension in a ⟨100⟩ direction. The diamonds indicate the orthorhombic path, and the circles indicate the tetragonal path.

TABLE II. The calculated ideal tensile strength and Young's moduli of Mo and Nb. For Nb, the ideal strength of the orthorhombic path is significantly smaller than that of the tetragonal path.

	Mo	Nb	
		Orthorhombic	Tetragonal
σ_m(GPa)	28.8	13.1	18.8
E_{100}(GPa)	370	165	165
σ_m / E_{100}	0.078	0.079	0.114

that fixed the saddle point in shear. But we are now approaching it from states of higher energy, so it provides a minimum in the energy along the tensile path. With respect to the ground bcc state, the tensile strains at which this special tetragonal structure appears in Mo and Nb are 0.454 and 0.493, and the perpendicular strains in Mo and Nb are -0.162 and -0.173, respectively.

The tetragonal Bain path is the path that was assumed in prior work on the ideal tensile strength of bcc crystals.[10,15,21] In the present study, we relaxed that constraint, and found the qualitative change in high strain behavior that appears in Figs. 5 and 6. The path taken during a relaxed tensile strain in the ⟨100⟩ direction branches away from the Bain path before the fcc structure is reached. The low-energy branch follows an ''orthorhombic'' path on which the strained crystal has a face-centered orthorhombic structure of the type shown in Fig. 7(c). The energy maximum along the orthorhombic path is the saddle point that is reached when the face-centered orthorhombic structure is strained into a stress-free tetragonal structure. This structure is the same tetragonal saddle-point structure that governs the ideal strength in shear and also appears at large strain along the tetragonal path.

After the strained crystal passes through the tetragonal structure on the orthorhombic path, its energy decreases monotonically with increasing tensile strain, reaching a minimum at a strain of $\epsilon = \sqrt{2} - 1 = 0.414$. At this strain, the structure has returned to bcc.

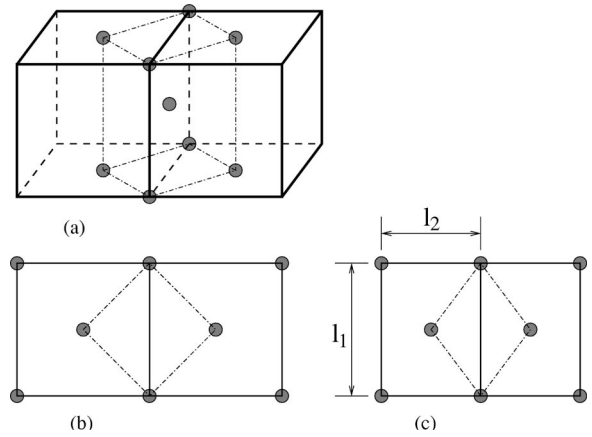

FIG. 7. Configurations along the tetragonal (Bain) and orthorhombic strain paths for a bcc crystal strained in relaxed tension in the [001] direction. (a) The strained configuration shown as a fct structure with a bct cell embedded in it. (b) and (c) The atom configuration in the basal (001) plane when the strain is tetragonal (b) or orthorhombic (c).

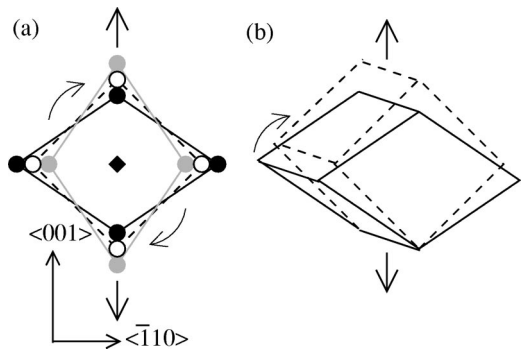

FIG. 8. The orthorhombic distortion under $\langle 001 \rangle$ tension, (a) the atomic configuration in the (110) plane, showing the initial bcc state in solid black, the bct saddle-point structure in dashed black, and the final bcc state in solid gray, and (b) the same picture in a perspective view, showing only the initial bcc structure and the bct saddle-point structure.

The orthorhombic path can be described as follows. Let the height of the orthorhombic cell, along the tensile axis, be $h=a_0(1+\epsilon)$, where a_0 is the edge length of the original bcc cell, and let the edge lengths of its base be l_1 and l_2, as in Fig. 7. The stress-free states along the orthorhombic path are

$$h=a_0,\ \ l_1=l_2=\sqrt{2}a_0 \quad \text{bcc},$$

$$a_0<h=l_2<l_1 \quad \text{tetragonal saddle point},$$

$$h=l_1=\sqrt{2}a_0,\ \ l_2=a_0 \quad \text{bcc}.$$

While the Bain path is a tensile stretch, the orthorhombic path can be understood as a shear deformation on the $\{211\}\langle 111\rangle$ slip system. This point is illustrated in Fig. 8, which shows the initial structure, the structure at the saddle point, and the regenerated bcc structure along the orthorhombic path generated by a relaxed tension on $\langle 100\rangle$. In each of these three configurations, the axis perpendicular to the plane of the figure is essentially unstrained. Also, by orthorhombic symmetry, there are no shears perpendicular to the plane of the figure. It follows that the the strain corresponds to a simple shear on the $(\bar{1}12)$ plane, which is oriented at 45° to the [001] direction in the saddle-point structure. Thus, if failure occurs on the orthorhombic branch it is not, strictly, a tensile failure along [001], but a shear failure on the $(\bar{1}12)\times[111]$ system at 45° to [001].

A relaxed tension in a $\langle 100\rangle$ direction always takes the tetragonal path in the limit of small strain; the two perpendicular $\langle 100\rangle$ directions are equivalent by symmetry and, hence, have the same elastic modulus. However, the tetragonal path ($l_1=l_2$) is simply a special case of the orthorhombic path ($l_1=l_2$ or $l_1\neq l_2$). Since the orthorhombic path provides an additional degree of freedom, it is not surprising that is preferred at larger strains. As Fig. 5 shows, in both Mo and Nb the deformation starts along the tetragonal Bain path, but branches away onto an orthorhombic path before reaching the fcc saddle point.

Whether the branch away from the tetragonal path affects the ideal tensile strength depends on when that branching occurs. As shown in Fig. 6, in Mo the deformation adheres to the tetragonal path until after the ideal strength has been reached. It follows that the orthorhombic distortion does not influence the ideal strength, and that Mo will fail in tension when pulled in the $\langle 100\rangle$ direction, at an ideal strength, $\sigma_m = 28.8\ \text{GPa} = 0.078\ \text{E}_{100}$, where

$$E_{100}=\frac{(C_{11}+2C_{12})(C_{11}-C_{12})}{C_{11}+C_{12}} \tag{4}$$

is the tensile modulus for a fully relaxed stretch along $\langle 100\rangle$.

In Nb, on the other hand, the branch occurs before the inflection point of the tetragonal deformation curve, and causes a significant decrease in the ideal tensile strength, from $\sigma_m = 18.8\ \text{GPa} = 0.114\ \text{E}_{100}$, the value predicted from the tetragonal path, to $\sigma_m = 13.1\ \text{GPa} = 0.079\text{E}_{100}$. At the same time, the failure mode changes from a tensile stretch to a shear on $\{211\}\langle 111\rangle$. Significantly, the resolved shear stress on the most favorably oriented $\{211\}\langle 111\rangle$ slip system when Nb fails in tension is very near 6.4 GPa, the ideal shear strength for this slip system, reinforcing the conclusion that the failure mode is not a stretch but a shear. Since the ideal shear strength is affected by the presence of other stresses, to a degree we have not yet explored for this system, we would not expect the resolved shear stress at failure to be exactly equal to the ideal shear strength.

IV. DISCUSSION AND CONCLUSION

The ideal shear and tensile strengths of Mo and Nb are presented in Tables I and II as well as the dimensionless strengths $\sigma^*=\sigma_m/E_{100}$ and $\tau^*=\tau_m/G_{111}$. While we know of no other calculations of the tensile strengths of Mo or Nb (other than our own preliminary results mentioned in Ref. 2), the ideal shear strengths for the $\{211\}\langle 111\rangle$ system were computed by Paxton *et al.*[12] and by Söderlind and Moriarty.[28] Their calculations neglected relaxation, and gave the results $\tau_m(\text{Mo}) = 17.8\ \text{GPa}$,[12] 20.9 GPa,[28] and $\tau_m(\text{Nb}) = 7.52\ \text{GPa}$.[12] Because these calculations neglected relaxation, the associated paths do not include the stress-free saddle points. They are therefore expected to predict somewhat higher ideal strengths, as they do.

In dimensionless terms, the tensile and shear strengths of Mo are almost identical to those of W (Ref. 15): $\sigma^* = 0.078$ (Mo), 0.071 (W); $\tau^* = 0.12$ (W and Mo). Both these numbers are close to the strengths that are inferred from simple models that assume a sinusoidal stress-strain relation from the bcc starting structure to the appropriate stress-free state.[2] We expect, therefore, that these results are typical for bcc metals.

While we know of no experimental data on the ideal tensile strength of Mo, the ideal shear strength may have been measured in nanoindentation experiments by Lilleodden and Nix.[29–31] Indentation on a sample surface produces a shear stress that has its maximum value some distance beneath the surface that is being indented. In nanoindentation the indenter is so small (50–1000 nm) that the subvolume that experiences high shear is likely to be defect free. The maximum shear stress at the onset of plastic deformation can be

computed from the indentation data and, in the case of Mo (and W), this shear stress is very close to the computed value of the ideal shear strength.[31]

While Mo behaves as expected, the behavior of Nb is anomalous. Its dimensionless shear strength, $\tau^* = 0.15$ is significantly higher than that of W or Mo, even though it is determined by the same stress-free state. Its dimensionless tensile strength $\sigma^* = 0.079$ is almost the same as that of W and Mo, even though it is determined by a very different saddle point. Its strength would be much higher if it followed the tetragonal path rather than branching off. Moreover, the stress-strain relations that govern shear and tension along the tetragonal path show clear deviations from sinusoidal shape; in both cases, the maxima in the stress occur at much higher strain than a sinusoidal form would predict.

As we mentioned at the beginning of this paper, one impetus for studying Nb was the small value of its shear modulus G_{111} relative to its tensile modulus E_{100}. The small value of this ratio suggests that an infinite perfect crystal of Nb would deform in shear before breaking in tension, even when pulled along $\langle 100 \rangle$. This is the behavior we actually find. In contrast to Mo, which fails in tension under the influence of the fcc saddle point, Nb branches to the orthorhombic path before failure, and thus fails in shear. Since our solution is appropriate for $T = 0$ K, this result suggests that Nb may not show the clean ductile-brittle transition via {100} cleavage that is common to the bcc transition metals. However, it is found experimentally that Nb does fail by {100} cleavage in fracture tests at low temperature.[32] The source of this cleavage is uncertain, but it may reflect the influence of the triaxial crack-tip stress state on the relative stresses for failure in $\langle 100 \rangle$ tension and {211} shear. This issue is under investigation.

ACKNOWLEDGMENTS

This work was supported by National Science Foundation Grant No. DMR-9520554, by the Director, Office of Energy Research, Office of Basic Energy Sciences, Materials Sciences Division of the U.S. Department of Energy, and by the Laboratory Directed Research and Development Program of Lawrence Berkeley National Laboratory under the U.S. Department of Energy. Computational resources have been provided by the National Science Foundation at the National Center for Supercomputing Applications and by the National Energy Research Scientific Computing Center, which is supported by the Office of Energy Research of the U.S. Department of Energy. All Department of Energy support was under Contract No. DE-AC03-76SF00098.

*Email address: wdluo@civet.berkeley.edu

[1] A. Kelly and N. H. Macmillian, *Strong Solids*, 3rd ed. (Clarendon Press, Oxford, 1986).
[2] J. W. Morris, Jr., C. R. Krenn, D. Roundy, and M. L. Cohen, in *Phase Transformations and Evolution in Materials*, edited by P. E. Turchi and A. Gonis (TMS, Warrendale, PA, 2000), p. 187.
[3] M. Polanyi, Z. Phys. **7**, 323 (1921).
[4] J. Frenkel, Z. Phys. **37**, 572 (1926).
[5] F. Milstein, J. Appl. Phys. **44**, 3825 (1973).
[6] F. Milstein, in *Mechanics of Solids*, edited by H. Hopkins and M. Sewell (Pergamon, Oxford, 1982), p. 417.
[7] F. Milstein and S. Chantasiriwan, Phys. Rev. B **58**, 6006 (1998).
[8] M. Šob, L.G. Wang, and V. Vitek, Mater. Sci. Eng., A **234–236**, 1075 (1997).
[9] M. Šob, L.G. Wang, and V. Vitek, Kovove Mater. **36**, 145 (1998).
[10] M. Šob, L.G. Wang, and V. Vitek, Philos. Mag. B **78**, 653 (1998).
[11] D. Roundy, C.R. Krenn, M.L. Cohen, and J.W. Morris, Jr., Phys. Rev. Lett. **82**, 2713 (1999).
[12] A.T. Paxton, P. Gumbsch, and M. Methfessel, Philos. Mag. Lett. **63**, 267 (1991).
[13] P.J. Craievich, M. Weinert, J.M. Sanchez, and R.E. Watson, Phys. Rev. Lett. **72**, 3076 (1994).
[14] P. Alippi, P.M. Marcus, and M. Scheffler, Phys. Rev. Lett. **78**, 3892 (1997).
[15] D. Roundy, C.R. Krenn, M.L. Cohen, and J.W. Morris, Jr., Philos. Mag. A **81**, 1725 (2001).
[16] J.W. Morris, Jr. and C.R. Krenn, Philos. Mag. A **80**, 2827 (2000).
[17] R. Hill, Math. Proc. Cambridge Philos. Soc. **77**, 225 (1975).
[18] R. Hill and F. Milstein, Phys. Rev. B **15**, 3087 (1977).
[19] F. Milstein, Solid State Commun. **34**, 653 (1980).
[20] D.M. Clatterbuck, D.C. Chrzan, and J.W. Morris, Jr., Philos. Mag. Lett. **82**, 141 (2002).
[21] C.R. Krenn, D. Roundy, J.W. Morris, Jr., and M.L. Cohen, Mater. Sci. Eng., A **319–321**, 111 (2001).
[22] J. Ihm, A. Zunger, and M.L. Cohen, J. Phys. C **12**, 4409 (1979).
[23] D.M. Ceperley and B.J. Alder, Phys. Rev. Lett. **45**, 566 (1980).
[24] J.P. Perdew and A. Zunger, Phys. Rev. B **23**, 5048 (1981).
[25] M.L. Cohen, Phys. Scr. **T1**, 5 (1982).
[26] B.G. Pfrommer, M. Côté, S.G. Louie, and M.L. Cohen, J. Comput. Phys. **131**, 233 (1997).
[27] *Landolt-Bornstein LBIII/29a-Low Frequency Properties of Dielectric Crystals: Second and Higher Order Elastic Constants*, edited by D. F. Nelson (Springer-Verlag, Berlin, 1992).
[28] P. Söderlind and J.A. Moriarty, Phys. Rev. B **57**, 10 340 (1998).
[29] E.T. Lilleodden and W.D. Nix (private communication).
[30] C. R. Krenn, Ph.D. thesis, Department of Materials Science and Engineering, University of California, Berkeley, CA, 2001.
[31] C.R. Krenn, D. Roundy, M.L. Cohen, D.C. Chrzan, and J.W. Morris, Jr., Phys. Rev. B **65**, 134111 (2002).
[32] C. Gandhi and M.F. Ashby, Acta Metall. **27**, 1565 (1979).